Clim Dyn (2007) 29:553–564
DOI 10.1007/s00382-007-0248-7

The climatic impact of supervolcanic ash blankets

Morgan T. Jones · R. Stephen J. Sparks · Paul J. Valdes

Received: 8 September 2006 / Accepted: 21 March 2007 / Published online: 22 May 2007

Abstract Supervolcanoes are large caldera systems that can expel vast quantities of ash, volcanic gases in a single eruption, far larger than any recorded in recent history. These super-eruptions have been suggested as possible catalysts for long-term climate change and may be responsible for bottlenecks in human and animal populations. Here, we consider the previously neglected climatic effects of a continent-sized ash deposit with a high albedo and show that a decadal climate forcing is expected. We use a coupled atmosphere-ocean General Circulation Model (GCM) to simulate the effect of an ash blanket from Yellowstone volcano, USA, covering much of North America. Reflectivity measurements of dry volcanic ash show albedo values as high as snow, implying that the effects of an ash blanket would be severe. The modeling results indicate major disturbances to the climate, particularly to oscillatory patterns such as the El Niño Southern Oscillation (ENSO). Atmospheric disruptions would continue for decades after the eruption due to extended ash blanket longevity. The climatic response to an ash blanket is not significant enough to instigate a change to stadial periods at present day boundary conditions, though this is one of several impacts associated with a super-eruption which may induce long-term climatic change.

M. T. Jones (✉) · R. S. J. Sparks
Department of Earth Sciences, University of Bristol,
Wills Memorial Building, Queens Road,
BS8 1RJ Bristol, UK
e-mail: morgan.t.jones@bristol.ac.uk

P. J. Valdes
School of Geographical Sciences, University of Bristol,
University Road, BS8 1SS Bristol, UK

Keywords Supervolcano · Super-eruption · Ash blanket · ENSO · Climate change

1 Introduction

Supervolcanoes are caldera systems capable of erupting in excess of hundreds to thousands of km^3 of magma in a single event. Examples include Yellowstone in USA, La Pacana in Chile and Toba in Indonesia. Large eruptions are classified on their total ejected mass (m) using a logarithmic magnitude scale, M (Pyle 1995; Pyle 2000). This is defined by: $M = \log_{10}(m) - 7.0$. Explosive super-eruptions are defined as M8 or larger by Mason et al. (2004). Eruptions of this magnitude are rare, with a minimum estimated frequency of 1.4 events Ma^{-1}, though multiple super-eruptions appear to occur in pulses of activity (Mason et al. 2004). A recent example of an eruption of this magnitude came from the Toba caldera in Sumatra around 74,000 years ago (Rose and Chesner 1987; Rampino and Self 1993; Zielinski et al. 1996; Oppenheimer 2002). Supervolcanoes are predicted to have large magma supply rates up to and possibly above 10^7 m^3 s^{-1} (Baines and Sparks 2005). Rapid injection of material into the atmosphere entrains and heats the surrounding air. The resulting effects of expansion and dilution significantly reduce the density of the eruption cloud and give the jet buoyancy. The cloud does not become buoyant immediately as the width of the vent prevents effective mixing of the atmosphere with the centre of the eruption column. This leads to column collapse and the formation of radial pyroclastic density currents. The deposits from these events are known as ignimbrites. Entrainment of air at the top of the flow and sedimentation of larger lithic (rock) fragments reduces the net density as the flow progresses. This allows the upper

part of the flow to become buoyant and rise (Sparks and Walker 1977; Sparks et al. 1986). There may be fluctuations in magma supply rates during ignimbrite formation, but observations from previous eruptions, theoretical work and experimental analysis suggest that the lift-off of a co-ignimbrite cloud is relatively abrupt and can therefore be assumed to act as a single cloud (Sparks et al. 1986; Sparks and Bonnecaze 1993; Sparks et al. 1997). The supply rates of ash and hot air into the rising plume are predicted to be 10^{11}–10^{13} m^3 s^{-1} (Baines and Sparks 2005). The ash forms an umbrella cloud when it reaches neutral buoyancy, predicted to be between 27 and 38 km above sea level at the peak of the eruption (Woods and Wohletz 1991; Rampino and Self 1992, 1993; Baines and Sparks 2005).

If ash umbrella clouds become over 600 km in diameter the rate of spreading becomes controlled by a balance between gravity and Coriolis forces (Baines and Sparks 2005). The ash cloud forms a spinning body that has nearly fixed proportions and is largely unaffected by stratospheric winds, allowing the cloud to spread out radially. The removal of ash by gravitational sedimentation in the days and weeks after the eruption creates a radial ash blanket around the vent. A typical super-eruption can expel around 1,000 km^3 of co-ignimbrite ash, enough to cover a continent the size of North America (~10^7 km^2) with a blanket of ash 100 mm thick.

2 Methodology and approach

Several processes in super-eruptions can severely disturb the ocean-atmosphere system. The most widely studied is the mass injection of ash, SO_2 and aerosols into the stratosphere. For example, the 74 ka Toba eruption is estimated to have ejected 10^{12}–10^{13} kg of volcanic aerosols and ash (Rampino and Self 1992). The effects of aerosols in the stratosphere have been highlighted as the primary mechanism for climate forcing on timescales of a few years (Rampino and Self 1992, 1993; Bekki et al. 1996; Zielinski et al. 1996; Carroll 1997; Robock 2000; Rampino 2002; Jones et al. 2005; Timmreck and Graf 2005). In particular, sulfuric acid aerosol scatters shortwave radiation and causes a net cooling of the Earth's surface (Bekki 1995; Robock 2000; Savarino et al. 2003; Jones et al. 2005; Timmreck and Graf 2005). Ash has a stratospheric residence time of a few weeks and long-term climatic effects from ash in the atmosphere are believed to be negligible. SO_2 has a slightly longer residence time as its removal is dependent on conversion to H_2SO_4 aerosol. Excessive SO_2 loading can potentially reduce OH levels, leading to stratospheric dehydration and an increased SO_2 lifetime by impeded H_2SO_4 conversion (Bekki 1995). However, stratospheric aerosol concentrations are lower as a result and the entrainment of tropospheric water has not been included in previous models. Timescales for the influence of a sulfate cloud depend on the post-eruptive hydration state of the stratosphere. Unrestricted atmospheric residence times for SO_2 are between 1 and 3 years (Robock 2000). If complete dehydration of the stratosphere should occur, the climate may be directly affected for several years longer (Bekki 1995; Bekki et al. 1996).

Volcanogenic processes capable of altering the climate on longer timescales include the deposition of ash on land. Vegetation proximal to the volcano will be buried by ash. 10 mm of ash is enough to disrupt most forms of agriculture and flora (Sparks et al. 2005). Plants and trees too high to be buried are often killed by the effects of acid rain and ash-leachates. Volcanic gases, metal salts and other volatiles erupted can be scavenged from the atmosphere by fine ash particles. These ash-leachates stay adsorbed onto the ash particle surfaces until removed by dissolution (Frogner et al. 2001; Witham et al. 2005). Temperatures in the stratosphere are too low to support liquid H_2O, so most of the ash-leachates will still be present on the particle surface when deposited, allowing them to be released into the surrounding environment. Toxic levels of aluminum (as AlF_x^{+3-x} complexes), fluoride and other compounds released by the ash induce ecosystem stress and species decline. This particularly affects systems with a low turnover rate, such as ponds, lakes and soils (Frogner 2004). Ecological sensitivity to ash-leachates depends on the ability of the ecosystem to buffer the effects. Though parent magmas of supervolcanoes are volatile-poor compared to basic magmas, a large-scale loading of ash per unit area will induce toxic and acidic conditions above most ecosystems' buffering capacity, killing flora that survived the burial phase. Such large-scale deforestation will interplay with the radiation budget, the carbon cycle and evapotranspiration.

Ecological responses to the 1883 eruption of Krakatoa (Indonesia) show that it took 5 years before grasses began re-colonizing affected islands and 15 years to re-establish trees and shrubs (Bush 2006). Evidence from the re-colonization of flora after the 1980 eruption of Mount St. Helens (USA) shows that pioneer species can become restricted or even halted by insect herbivory (Fagan and Bishop 2000; Bishop 2002; Knight and Chase 2005), further lengthening the recovery of flora after an eruption. To our knowledge there are no studies of the decline in flora following a super-eruption, but the response is likely to last for much longer as re-colonization of pioneer species requires seeding by either wind or animal transport. The scale of the deposits dictates that the recovery of flora must

do so from the edges and heavily eroded areas of the ash blanket. Climatic responses to vegetation loss may also hamper the recovery of flora. Therefore, it is likely that an area in the region of 3×10^6 km^2 would be completely devoid of plant-life following a super-eruption for well over a decade.

A continental sized ash blanket will interplay with the surface radiation budget and therefore interact with atmospheric circulation. Volcanic ash is extremely reflective due to large concentrations of silica rich glass and high particle vesicularity. As a result, an ash blanket will significantly increase the surface albedo. This will reflect a greater proportion of incoming radiation, leading to surface cooling. Some tephra deposits have albedo values comparable to snow. Thus the albedo effects of a continental ash blanket are comparable to those of an ice sheet. Surface cooling could also initiate the build up of snow and ice on top of the ash blanket, amplifying the initial albedo forcing.

Residence times of ash blankets at the surface are aided by the rapid establishment of stable channel and rill (rivulet) networks, decreasing the erodibility of the tephra layer (Collins and Dunne 1986; Leavesley et al. 1989). Co-ignimbrite ash is cohesive, inhibiting transportation by water and increasing surface runoff (Nammah et al. 1986). A mortar like crust is formed by desiccation, restricting erosion after the first couple of years to the channel and rill sides. For example, erosion of tephra from the 1980 eruption of Mount St. Helens slowed from 26.0 to 1.8 mm/year within 3 years (Collins and Dunne 1986). The scale of supervolcanic ash deposits should increase the residence time by at least an order of magnitude. Ash blanket lifetimes should be further aided by changes in the hydrological cycle. Surface cooling effects associated with the aerosol forcing reduce both evaporation rates and the saturation mixing ratio of water vapor in air. Modeling of such effects at a high sulfur loading show a halving of average initial global rainfall after an eruption (Jones et al. 2005). A reduction in precipitation will in turn reduce the erosion rate of the ash blanket. Studies of sedimentary and geomorphic responses to ignimbrite sheet emplacement suggest that a large ash blanket could exert a significant environmental influence for considerably more than 10 years following an eruption (Manville 2002). A possible negative feedback is the impact of larger volumes of snow from aerosol induced cooling, which would melt during spring and increase erosion. Though the lifetime of an ash blanket is difficult to constrain and the removal of ash at the surface would be gradual, we surmise that an ash blanket will remain a significant climatic forcing for at least 10–50 years after an eruption. The impact of an ash blanket is likely to alter the climatic responses predicted by models only dealing with the effect of aerosols and is therefore an important consideration.

3 Climate model and experimental design

To assess the impact of a known supervolcano, we conducted a climate sensitivity experiment by simulating the effects of an ash blanket from an eruption of the Yellowstone Caldera in Wyoming, USA, using the Hadley Centre coupled atmosphere-ocean model, HadCM3 (Gordon et al. 2000; Pope et al. 2000). This is a well-known General Circulation Model (GCM) that has been used to successfully predict past and present climatic conditions (Stott et al. 2000; Hewitt et al. 2001; Tett et al. 2002) and is widely used for future predictions (e.g. Johns et al. 2003). Our control simulation is for pre-industrial conditions (CO_2 = 290 ppmv, solar irradiance = 1,365 W m^{-2}). We use the Meteorological Office Surface Exchange Scheme (MOSESII), which represents the transfer of heat, momentum, moisture and carbon between land and atmosphere. The atmosphere has a horizontal resolution of 2.5° by 3.75° and has 19 vertical levels. The ocean has a horizontal resolution of 1.25° by 1.25° and 20 vertical levels. We have based the modeled ash blanket on ashfall from the 2 and 0.64 Ma eruptions of Yellowstone caldera (Fig. 1) (e.g. Reynolds 1975; Perkins and Nash 2002; Sparks et al. 2005). This involved two alterations to the model set-up; the vegetation coverage and the soil albedo. Based on the inferences from smaller eruptions, we have assumed complete destruction of vegetation for an area of 3×10^6 km^2, labeled the Inner Zone in Fig. 1. In the larger Outer Zone (~7.56×10^6 km^2) 50% of flora is removed,

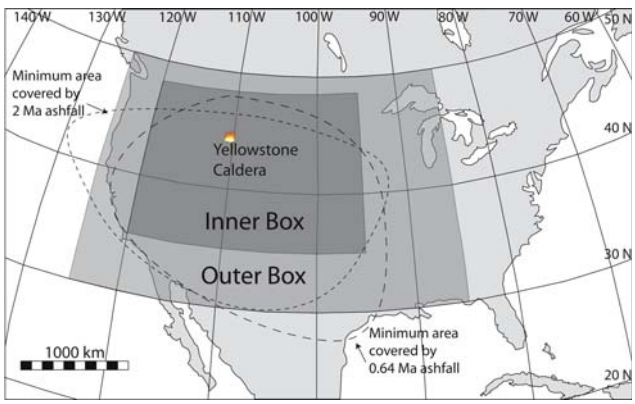

Fig. 1 Map of North America illustrating the known ashfall from two eruptions of Yellowstone and the affected area in the ash blanket simulation. The *shaded areas* show the 'two box' configuration assumed by the model. For the *inner box*, total destruction of vegetation is assumed. The soil values in the model are replaced with the physical properties of ash. The distal *outer box* suffers a 50% reduction in flora. Soil properties for the outer box are an average between ash and the original soil. The two *dashed lines* enclose sites where previous ash deposits have been recognized (e.g. Sparks et al. 2005). The actual area covered by ash is likely to have been significantly larger

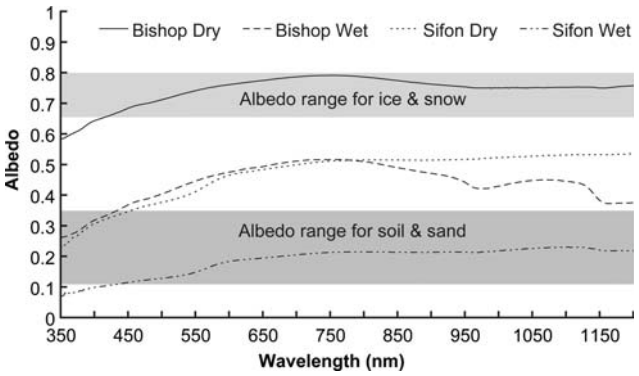

Fig. 2 Albedo ranges of ash. Dry and wet samples from the Sifon Ignimbrite (Chile) and the Bishop Tuff (USA) were analyzed by spectroscopy. For the wet samples, water was added till the ash reached saturation then a paper towel was dabbed to remove excess surface water. This gives end member values for degree of wetness for ash samples

while maintaining the ratios between original vegetation types.

The bare soil albedo is the model representative of the reflectivity of the ground where there is no water or vegetation coverage. To ascertain a suitable input parameter, measurements of ash albedo were made using dry and wet samples from the Bishop Tuff, USA and the Sifon Ignimbrite, Chile (Fig. 2), two deposits from previous supervolcanic eruptions. The two ash samples can be considered end members in the albedo range for supervolcanic ash, with the Bishop Tuff more comparable to tephra from Yellowstone as it is a co-ignimbrite ash sample of similar composition. The Sifon Ignimbrite is a deposit from pyroclastic density currents which have a greater component of lithic and crystalline material, reducing the albedo. Reflectivity between 350 and 1,200 nm is averaged by spectroscopy to give a mean albedo as the model requires a single number as an input parameter. Dry Bishop Tuff ash has the highest albedo value of 0.74, equivalent to fresh snow and much higher than typical values for soils and sand (0.1–0.35). Figure 2 illustrates the dependency of albedo on the degree of wetness, suggesting a complicated feedback mechanism between surface albedo and the hydrological cycle. Soil albedo is not a function of soil moisture in HadCM3 so we chose an albedo value of 0.47, the mean of all samples measured and the suggested method for modeling all soils except for semi-arid and desert environments (Wilson and Henderson-Sellers 1985). While the effects of an ash blanket may induce semi-arid conditions, taking the average of dry and wet samples will at worst underestimate the mean surface albedo. Additional experiments using an Atmospheric General Circulation Model (AGCM) with a slab ocean were run to test the sensitivity of the model to changes in albedo (see Model Sensitivity, Chap. 4.4).

The aim of this study is to isolate the potential impacts of a supervolcanic ash blanket and assess the climatic sensitivity to a terrestrial forcing unrelated to the effects of stratospheric aerosols. It is therefore a sensitivity experiment and is not aimed at reproducing a specific super-eruption. The simulations do not include the effects of stratospheric loading of aerosols on the climate, allowing the effects of the ash blanket to be clearly recognized. Excluding the effects of initial stratospheric loadings means the starting conditions of the simulations do not reflect the true initial conditions after a super-eruption, such as increased snow cover and a reduction in radiative forcing. Further work will need to couple the effects together to investigate non-linear feedbacks. For these experiments, a transient analysis of the climatic response seems inappropriate. Instead, it is assumed that the lifetime of the ash blanket is of sufficient length to outlast the aerosol induced effects and to allow a temporary climatic steady-state to develop. This model sets out to predict what these steady-state conditions will be following the relaxation of the sulfur loading. The control and altered simulations are started from the spun-up control run. In the altered simulation affected by ash, emplacement of the blanket is assumed to be instantaneous. The model then simulates 200 years of ashfall affected atmospheric and ocean circulation. The first 20 years are discounted as the spin-up phase, where the system is trying to attain a new equilibrium. The following 180 years are then averaged to give mean altered climatic conditions. The same procedure is followed for the control run, allowing comparisons to be made between the two. This does not assume that the ash blanket residence time is 200 years, nor that vegetation growth will remain static during this period. The length of the simulation is purely to increase the signal to noise ratio (SNR) in response to the forcing. The key results from our simulation establish themselves relatively quickly and are noticeable within a decade. Plots of model responses show values at the 95% confidence level, based on the student's *t* test. This method approximates regions of statistical confidence but is limited due to issues of temporal and spatial autocorrelations. All of the major features in the results are identified at the 99% confidence level.

4 Results

4.1 Circulation and temperature response

The presence of an ash blanket induces large deviations from control conditions. Surface temperatures show significant local variations of ±5°C with only a 0.1°C decrease on a global scale compared to the control run. The localized character of the response is also true of precipitation,

evaporation and cloud cover. The globally averaged change in radiative forcing due to the imposed ash albedo was calculated using the method of Gregory et al. (2004). This showed that the instantaneous change was 1.0 W m^{-2} and that the model regained energy balance within the 200 years of the simulation. Locally over the ash blanket, the initial change in net top-of-the-atmosphere outgoing solar radiation is approximately 32 W m^{-2}. The combination of deforestation and an increase in albedo instigates local surface cooling exceeding 5°C throughout the year in North America, well outside the natural variability of the control model (Fig. 3). Surface cooling leads to higher surface pressures, especially during June, July and August (JJA), as increased insolation strengthens the absolute albedo effect (Fig. 4). The local decrease in temperature in North America changes the temperature gradient with the adjacent North Pacific. The heat stored by the ocean warms the atmosphere during December, January and February (DJF), causing an increase in baroclinic instability and the formation of more frequent and/or deeper low-pressure systems over the North Pacific (based on band passed filtered eddy kinetic energy, not shown). A greater response is observed during JJA due to the peak in relative surface cooling in North America at maximum insolation. Changes in pressure interplay with the northern hemisphere jet streams. The simulation results indicate a latitudinal shift of storm tracks in both the North Pacific and the North Atlantic Oceans (based on band pass filtered eddy kinetic energy). Comparisons of the perturbation to the stream function at 200 hPa between the altered simulation and the control suggest southwards movement in the North Pacific and northwards movement in the North Atlantic. In the North Pacific the storm track is amplified by up to 5 m^2 s^{-1}, presumably due to less frequent blocking by high-pressure systems. As a consequence slightly warmer conditions are promoted in northern North America compared with the control (Fig. 3).

The Pacific/North American teleconnection pattern (PNA) is affected by the surface perturbation in North America. The PNA is closely linked to the El Niño Southern Oscillation (ENSO) and variability in ENSO region 3.4 shows a consistent increase in inter-annual variability of sea surface temperatures (Fig. 5). HadCM3 is considered relatively accurate at mimicking natural vari-

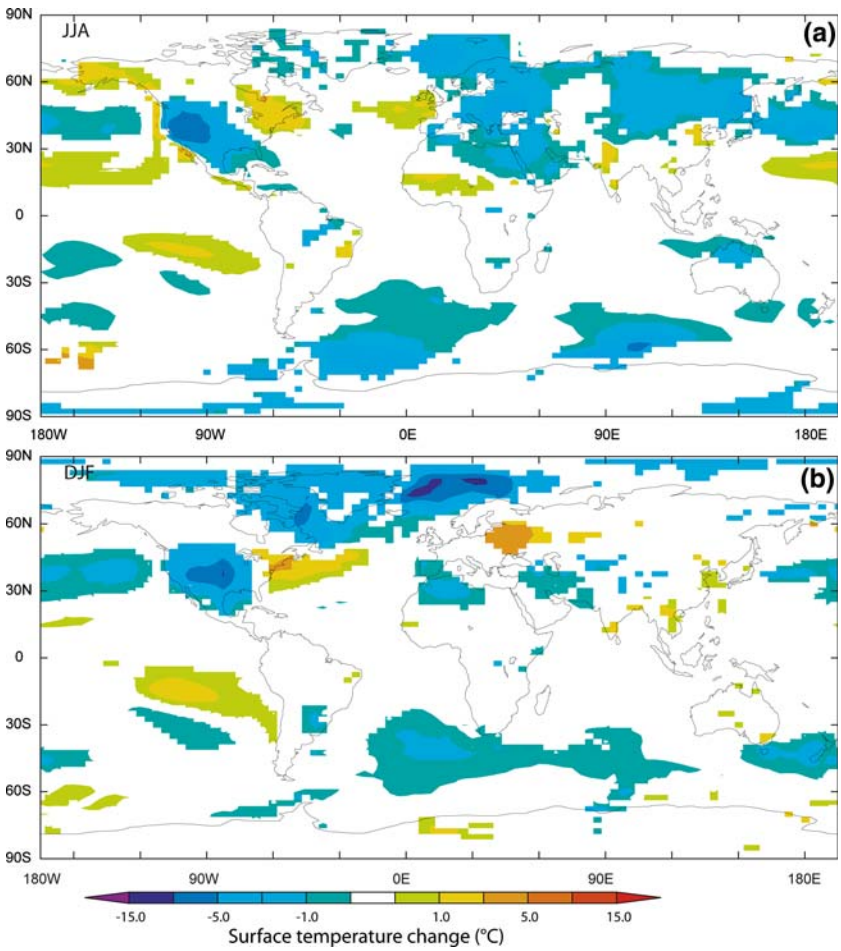

Fig. 3 Comparisons of surface air temperature between the ash-affected simulation and the control run (°C), showing anomalies exceeding the 95% statistical confidence level using the student's *t* test. **a** Show the global temperature changes for JJA and **b** highlights the temperature difference during DJF

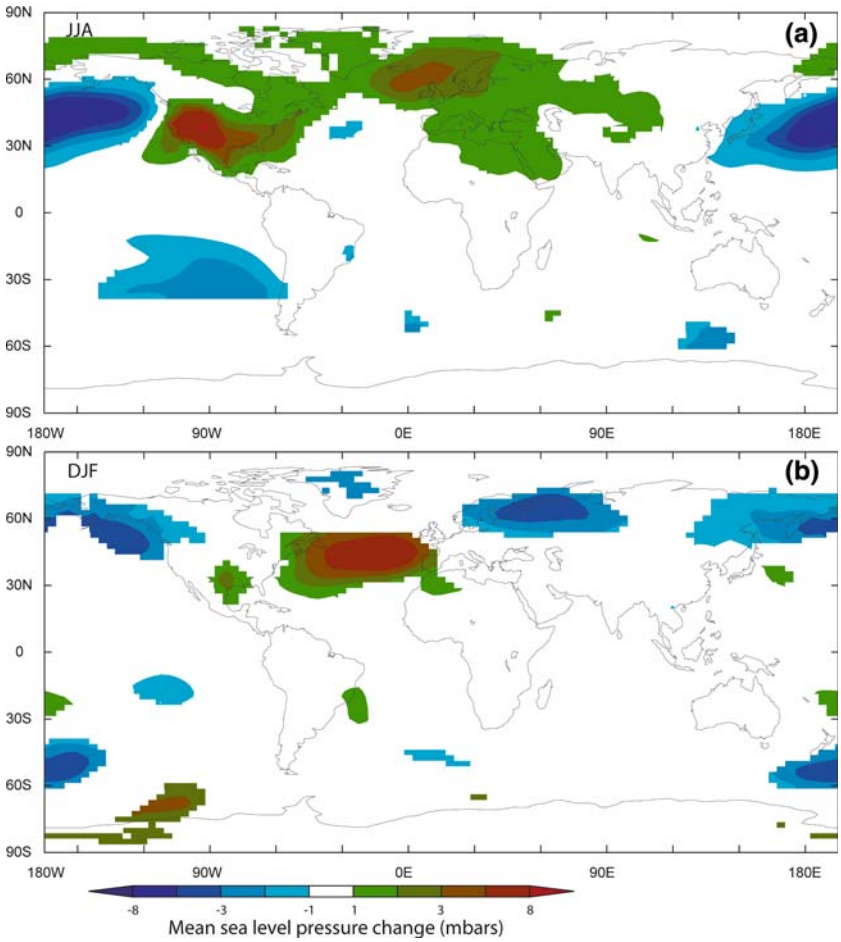

Fig. 4 Comparisons of mean sea level pressure between the altered run and the control run (mbars), showing anomalies exceeding the 95% statistical confidence level using the student's *t* test. **a** Shows conditions during JJA and **b** shows the change during DJF. High latitude pressures increase during summer months and decrease during winter months in both hemispheres

ability in ENSO (Collins 2000; Collins et al. 2001). Variability rises by more than 25% in all months, reaching a maximum of a 60% increase in December. The dominant change in ENSO variability is the magnitude of El Niño and La Niña events, with mean monthly sea surface temperatures ranging from 23 to 29°C in ENSO region 3.4 (Fig. 6). Enhancement of ENSO variability is not matched by large changes in eastern Equatorial Pacific surface temperatures (Fig. 3), so increases in frequency and/or magnitude of El Niño events are offset by La Niña episodes. The Southern Oscillation Index (SOI) provides another indicator of changes to ENSO by comparing the mean pressure changes for Tahiti and Darwin (Australia), with negative values suggesting a bias towards El Niño phases. Mean pressures drop in Tahiti from 1,009.9 to 1,009.5 mbar ($2\sigma = 1.0$) and rise in Darwin from 1,003.6 to 1,006.7 mbar ($2\sigma = 1.3$), combining to give a ΔSOI of –3.5. This suggests the ENSO signal does show greater or more frequent El Niño phases. Model predictions of ENSO should be treated with some caution due to large decadal and centurial variations in variability and differing responses of climate models to climate forcings (Collins 2000). However, the large magnitude of the response to an ash blanket gives us confidence in the validity of our results.

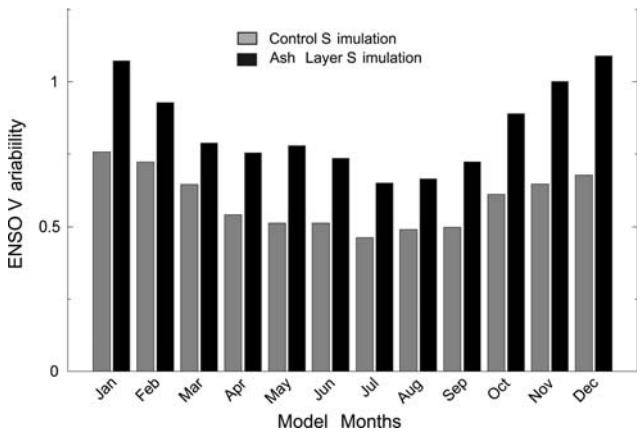

Fig. 5 Comparisons of surface temperature variability in ENSO region 3.4 between the control run and the altered simulation. The minimum rise in variability is in August (25%) and maximum variability occurs in December (60%)

The changes in the atmospheric circulation have significant repercussions throughout the globe. Northern

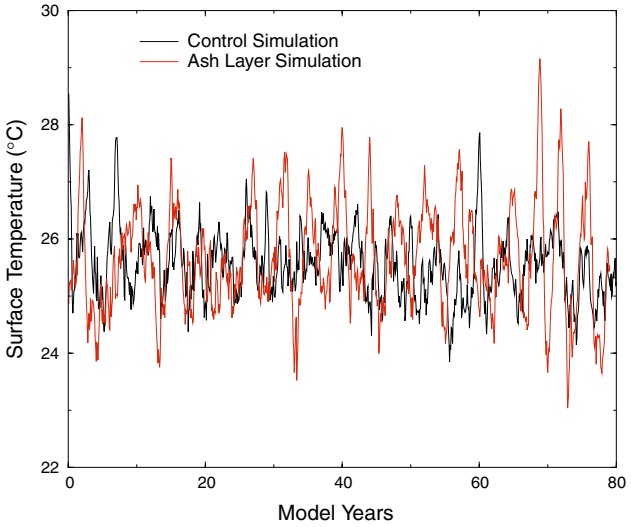

Fig. 6 Surface air temperatures for all months of the run in ENSO region 3.4, with the mean seasonal cycle removed. The increase in ENSO variability is dominated by an increase in El Niño and La Niña magnitudes. Extended periods of 'normal' circulation conditions are much less frequent in the ash layer simulation

hemisphere continents unaffected by ash burial are warmed by the increase in the advective effects transporting heat from the oceans to the continents. The warming is slight, so only certain areas such as northwest Russia and northeast USA see temperature increases outside the natural variability of the system (Fig. 3). However, there is sustained cooling of northern hemisphere continents during JJA that is greater than the 95% statistical confidence range. The Middle-East, northeast Africa and Eurasia all display 1°C cooling in response to changes in atmospheric circulation. There are significant changes in surface temperature and mean sea level pressure in the southern hemisphere, but these are restricted to oceans.

4.2 Ocean response

Ocean surface temperatures also react to the ash blanket forcing, though to a lesser degree than the atmospheric response. The Norwegian Sea shows a consistent and sustained cooling, where temperatures are consistently 1°C colder than the control. This should lead to large and sustained increases in sea ice. Svalbard (Norway) experiences a 42% increase in mean sea ice cover to 76.8% from the control value of 34.9% during DJF (2σ = 30.8). Further south, temperatures are influenced by the strengthening of the North Atlantic Thermohaline Circulation (NATHC). Overturning circulation shows a uniform increase from 16.8 to 19 Sv throughout the 200 year simulation, raising ocean temperatures by 2°C around Newfoundland throughout the year and by 1°C around the British Isles during JJA. Winter ocean temperatures in the equatorial Pacific are raised by 1–2°C in response to the increase in ENSO variability, supporting the suggestion of a slight bias towards El Niño episodes in ENSO. There is a comparable decrease in eastern North Pacific temperatures in response to the rearrangement of atmospheric circulation. Elsewhere ocean surface temperatures are relatively unaffected and show no long-term trends through the length of the simulation.

4.3 Precipitation response

Global precipitation patterns are modified by the changes in atmospheric circulation. In North America precipitation is reduced by over 2 mm/day during JJA from an average of 2.68 mm/day (Fig. 7). Evapotranspiration accounts for around 21% of precipitation recycled in the Mississippi Basin (Trenberth 1999), so the loss of vegetation accounts for some of the decrease. A reduction in the latent heat flux associated with deforestation slows the hydrological cycle. Other factors include the increase in surface pressures stabilizing the atmospheric boundary layer, possibly by reducing the air mass internal convection, which aids the reduction in precipitation. Precipitation in North America is less affected during DJF, which significantly increases snowfall due to the sustained drop in temperature. Recurrent snowfall covers large expanses of the ash blanket from November to April. The North American mean snow cover is greater than 50 cm thick above 40°N and the surface albedo suggests that the entire ash blanket is covered during February. The enhanced snow cover provides a positive feedback to the surface albedo increase and the subsequent impact on atmospheric circulation.

Around the Tropic of Cancer there is a general decrease in precipitation on continents, with Central America, the Sahel and Southeast Asia all seeing rainfall drop by around 1 mm/day during JJA (Fig. 7). The reduction in precipitation around the Bay of Bengal is probably attributed to the influence of ENSO on the Indian Monsoon, though the teleconnection is not a stable one. The strength of the monsoon is often diminished during El Niño years, so the reduction in precipitation in Southeast Asia may well be linked to the slight preference to El Niño phases in ENSO. The changes in the Americas and Africa are more difficult to explain, but are most likely to be in response to summer cooling of mid- to high-latitude continents. Monsoonal weather patterns gain strength from the temperature gradient between land and ocean, so a summer cooling of continents serves to reduce the strength of tropical weather systems. The precipitation decreases exceed the maximum variance of the system over much of Africa and India, suggesting an increase in drought frequency (Fig. 7a). During DJF the precipitation changes over the continents are much smaller (Fig. 7b). The main reason for the dis-

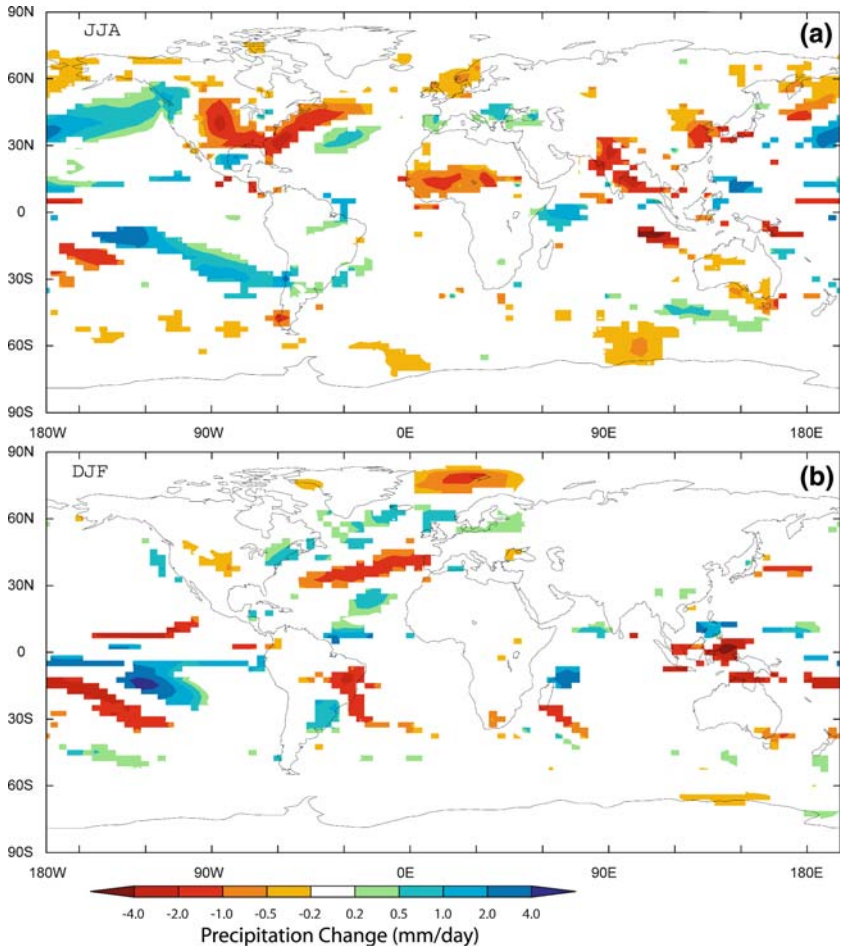

Fig. 7 Comparisons of mean precipitation between the ash-affected simulation and the control run (mm/day), showing anomalies exceeding the 95% statistical confidence level using the *F* test. **a** Show the global precipitation changes for JJA and **b** shows the precipitation difference for DJF

crepancy between the seasons is the positioning of the continents. Maximum insolation during DJF is in the southern hemisphere, where there are less continental land masses. Changes in seasonal temperature fluctuations affect continents more than oceans, so the impact on continental precipitation patterns during DJF is not as severe. In contrast, ocean precipitation patterns are affected throughout the year. Increases of over 2 mm/day 10° north and south of the equator are observed all year in the Pacific in response to increases in ENSO variability and changes to either the position and/or variability in the position of the Inter-Tropical Convergence Zone (ITCZ).

4.4 Model sensitivity

We conducted a series of simplified model simulations in order to assess the sensitivity of the results to vegetation loss and albedo increase. Due to computing time constraints the test runs used a slab ocean model (HadSM3) with the same atmospheric model component in HadCM3. These simulations simplify the calculations by assuming a thermodynamic ocean with predefined circulation and heat transport. Atmospheric responses to an ash blanket in HadSM3 compare well to those derived from the HadCM3 simulation. The only major exception is the response of the equatorial Pacific, where the ash blanket forcing manifests a response similar to ENSO by raising the surface air temperatures by 5°C in the slab ocean models as opposed to increasing ENSO variability (Fig. 8). The slab model is incapable of reproducing changes in oceanic overturning, but the increase in equatorial surface air temperatures suggests that it picks up the atmospheric forcing that interacts with ENSO in the coupled model. While the style of the response is comparable to the coupled model, the slab model appears to exaggerate the magnitudes of changes. Three experiments were conducted at varying albedo values to compare with a control simulation. Run α had an ash blanket albedo of 0.47, run β slightly lower at 0.36 (the average value for Sifon ash, Fig. 2) and run γ used the original soil input parameters to assess the impact of vegetation loss alone.

The results suggest that both albedo increase and vegetation loss are important climate forcings. DJF temperatures in North America drop by over 6°C in all three simulations, regardless of surface albedo (Fig. 8). Vegetation removal exposes bare earth and reduces surface heat

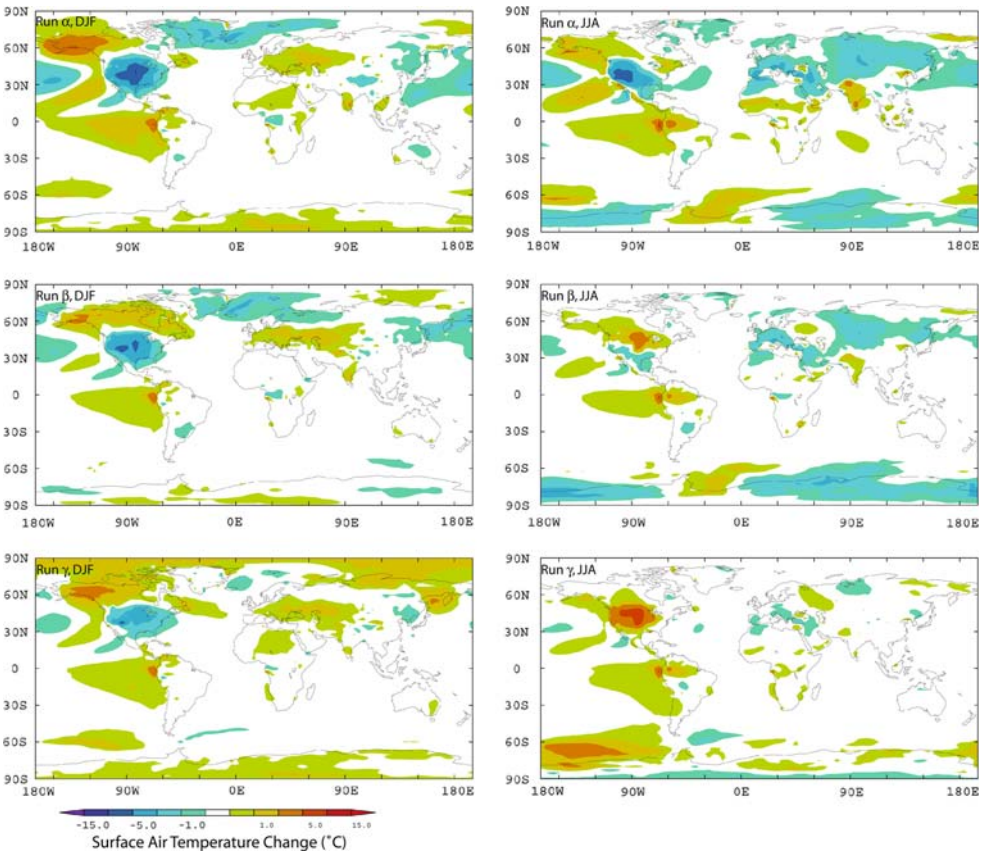

Fig. 8 Comparisons of mean surface air temperature change between HadSM3 simulations. *Row 1* shows run α, with an ash blanket albedo of 0.47. *Row 2* shows run β with an albedo of 0.36. The *3rd row* shows the results of run γ, which only simulates the removal of vegetation and keeps the original model surface albedo values. The *left* column is the average of DJF, the *right* column the mean of JJA months in the runs

retention. In response, the surface albedo during the winter increases through sustained snow accumulation above that of the control. This mechanism seems to be the dominant forcing, as the climatic response in run γ during DJF is very similar to the other two models. In contrast, the model responses during JJA are sensitive to surface albedo. In run γ, the planetary albedo over North America during JJA is lower than the control through exposure of dark soils and a reduction in cloud cover over North America. Changes in albedo are insufficient to explain adequately the rise in North American surface temperatures in run γ however, which peak at 9°C above the control (Fig. 8). The main reason for different responses is attributed to the interaction of evapotranspiration losses and surface albedo. Vegetation loss effectively reduces atmospheric moisture supply. The mean latent heat flux in central North America decreases from 140–160 W m^{-2} in the HadCM3 control to 20–40 W m^{-2} in the HadCM3 ash-affected simulation, also observed in the three simplified simulations. The large decrease in latent heat flux leads to surface heating during maximum insolation through elevated convective heating, as seen in run γ. The prevalence of a net surface cooling in run α and the main coupled simulation during JJA suggests that the surface cooling from the increase in surface albedo overprints the surface heating from the reduction in latent heat flux. Run β appears to be a combination of the processes, with net surface heating above 35 N and net cooling further south. This suggests that a high surface albedo becomes dominant in areas or times of greater insolation. Overall the similarities in DJF weather conditions between runs α, β and γ suggest that the effects of vegetation loss dominate in winter conditions (Fig. 8). Increases in surface albedo only dominate the local response during maximum insolation (JJA).

Overall the sensitivity experiments imply that both increased surface albedo and vegetation loss instigate a large climatic response. Varying the surface albedo does not result in large annual global changes in temperature, but does affect temperature variability in the vicinity of the ash blanket. A high surface albedo has the greatest impact during periods of high insolation and at low latitudes. The net impact is local cooling, initiating a global response. Combined, the effects of vegetation loss and albedo increase have a large impact on circulation patterns without dramatically changing the global temperature. These sensitivity studies highlight the difficulty in accurately assessing the transient response to a super-eruption. In the first few years after a super-eruption one would expect the influence of vegetation loss to dominate over the albedo increase due to reduced radiative forcing, but both processes are likely to be minor compared to the effect of stratospheric aerosols. If the erosion of the ash blanket

exceeds the rate of vegetation recovery, one would expect a transient change in climatic forcing from conditions predicted by run α to those calculated by run γ.

5 Discussion and conclusions

This study has investigated the volcanogenic forcing due to ash covering a continent sized area. The residence time of the ash blanket is expected to be decades and thus capable of perturbing climate well beyond the few first few years, when the effects of aerosols are likely to be dominant. A simulated ash blanket from Yellowstone has a significant impact on atmospheric circulation. The global climate does not change significantly in the ash-affected simulation, but seasonal climatic variability is substantially increased. Our findings, such as the change in ENSO variability and magnitude, are significant enough to impact climatic responses to other volcanogenic forcings.

Our choice of supervolcano location and initial starting conditions may affect climatic response. Similarly, the response may be somewhat different if the ''background'' climate was equivalent to past eruptions from Yellowstone (e.g. 0.64 or 2 Ma), but we suggest that our results showing the climatic importance of an ash blanket will be robust across all time periods. Ash blankets from eruptions at low latitudes will favor albedo induced surface cooling, while mid-to high latitude eruptions will be affected by seasonal responses with changes in latent heat flux associated with vegetation loss playing a more dominant role. Yellowstone is situated close the Pacific. Thus, the marked ENSO response to an ash blanket may be unique to North American supervolcanoes. The starting conditions are another caveat to the model response. The decision to use a pre-industrial control makes this sensitivity study applicable to the climatic response during a warm interglacial period. Initial ocean circulation is also an important starting parameter, especially given the response of the NATHC.

The climatic response to a continental ash blanket is less severe than those predicted for stratospheric sulfur loading. The response to a sulfate cloud from a Toba sized eruption is predicted to be global cooling between 3 and 10°C (Rampino and Self 1992, 1993; Rampino 2002; Jones et al. 2005). The climate sensitivity to an ash blanket does not include lasting effects from feedbacks other than those investigated here. There are several volcanogenic processes that could destabilize the climate prior to the appearance of effects caused by the ash blanket. Massive cooling events can dramatically affect ecosystems and flora. An increase in hard freezes will destroy significant amounts of vegetation (Rampino and Ambrose 2000). Further loss of biota will instigate a large climatic response as the model appears particularly sensitive to changes in vegetation cover. Changes in atmosphere chemistry following a super-eruption will also affect the response. Any changes in stratospheric chemistry would impact on sulfate concentrations and lifetimes, and may also affect changes in cloud cover. The aerosol induced temperature anomaly is predicted to be 2°C below normal 10 years after the eruption and 0.3°C cooler after 50 years from (Jones et al. 2005). If these predictions are correct, the steady-state climate predicted by our model will be slightly cooler, though this will aid the ash blanket residence time by slowing the hydrological cycle.

The impact of cooling on the hydrological cycle has further implications for the climatic response than just ash blanket longevity. The NATHC almost doubles in intensity in response to increased salinity and amplification of cooling at high latitudes (Hewitt et al. 2001; Luder et al. 2003; Jones et al. 2005). Our results have shown a similar NATHC response on a smaller scale, which would act as a positive feedback to the predicted aerosol induced increase in overturning. The promotion of sea ice formation in the Labrador and Norwegian Seas is likely to accentuate the response of the NATHC, though the expansion of sea ice will also decrease high latitude evaporation. The perturbation of the NATHC is predicted to last for 20 years from an aerosol forcing (Jones et al. 2005), but the effects of an ash blanket may heighten the intensity and longevity of the response, maintaining the NATHC as a negative feedback to the global cooling and buffering temperature decreases in western Europe.

Supervolcanoes have been implicated as possible catalysts for longer term climate change during periods of climatic instability (Rampino and Self 1992, 1993; Ambrose 1998; Rampino and Ambrose 2000), though this is contentious (e.g. Oppenheimer 2002; Lee et al. 2004). It was suggested that global cooling significantly increases snow and ice cover, raising the surface albedo and providing a positive feedback to the volcanic cooling. The response to an aerosol forcing predicts that the decrease in temperatures are insufficient to initiate a glaciation independently (Jones et al. 2005). A prolonged ash blanket raises the surface albedo considerably and increases snow and ice cover over North America in winter. It is possible that the combination of the ash blanket and the aerosols may allow persistent snow cover and encourage the expansion of ice sheets, but the study of their isolated impacts appears to be inadequate to achieve this. A long ash blanket residence time may instigate a stable change to the ocean-atmosphere system (Pollack et al. 1976) and amplify the initial forcing (Zielinski et al. 1996), but the scale of disruption still seems less than required. Other volcanogenic forcings such as changes in atmospheric chemistry, soil respiration and the planktonic response to both cooling and the addition of nutrients adsorbed onto

ash particles may be capable of initiating a long-term climatic response, either solely or combined with other feedbacks, but these have not been studied in detail. Climate variability may also dictate that long-term climate change is only achievable at certain times, possibly during susceptible periods of Milankovich cycles. It is also plausible that the stresses of glacial buildup and rapid melting may act as a cause, rather than an effect, to supervolcanism (Zielinski et al. 1997). Explosive super-eruptions occur too frequently to be solely responsible for mass extinction events or to be able to completely destroy continental ecosystems. They will, however, create a significant disruption to the climate in the short-term and possibly over longer timescales. We hope to extend our studies to include these effects.

Acknowledgments M.T.J. is funded by a NERC studentship. R.S.J.S. is supported by a Royal Society Wolfson Award. Thanks to the NERC Field Spectroscopy Facility at the University of Edinburgh for use of equipment and the NERC Centre of Atmospheric Sciences for high performance computer time. Thanks to Peter Baines, Vernon Manville, Jessica Trofimovs, Matthew Watson, Fred Witham and three anonymous referees for helpful comments.

References

Ambrose SH (1998) Late Pleistocene human population bottlenecks, volcanic winter, and differentiation of modern humans. J Human Evol 34:623–651

Baines PG, Sparks RSJ (2005) Dynamics of giant volcanic ash clouds from supervolcanic eruptions. Geophys Res Lett 32:L24808

Bekki S (1995) Oxidation of volcanic SO_2: a sink for stratospheric OH and H_2O. Geophys Res Lett 22(8):913–916

Bekki S, Pyle JA, Zhong W, Toumi R, Haigh JD, Pyle DM (1996) The role of microphysical and chemical processes in prolonging the climate forcing of the Toba eruption. Geophys Res Lett 23(19):2669–2672

Bishop J (2002) Early primary succession on Mount St Helens: impact of insect herbivores on colonizing lupines. Ecology 83:191–202

Bush MB (2006) Ecology of a changing planet, 3rd edn. Prentice Hall, New Jersey

Carroll MR (1997) Volcanic sulfur in the balance. Nature 389:543–544

Collins M (2000) Understanding uncertainties in the response of ENSO to greenhouse warming. Geophys Res Lett 27(21):3509–3512

Collins BD, Dunne T (1986) Erosion of tephra from the 1980 eruption of Mount St. Helens. Geol Soc Am Bull 97(7):896–905

Collins M, Tett SFB, Cooper C (2001) The internal climate variability of HadCM3, a version of the Hadley Centre coupled model without flux adjustments. Clim Dyn 17(1):61–81

Fagan W, Bishop J (2000) Trophic interactions during primary succession: herbivores slow a plant reinvasion at Mount St. Helens. Am Nat 155:238–251

Frogner P (2004) Al-F toxicity contributes to ecosystem stress and species decline following large-scale volcanism. Geochim Cosmochim Acta 68(11):A147

Frogner P, Gíslason SR, Óskarsson N (2001) Fertilizing potential of volcanic ash in ocean surface water. Geology 29(6):487–490

Gordon C, Cooper C, Senior CA, Banks H, Gregory HM, Johns TC, Mitchell JFB, Wood RA (2000) The simulation of SST, sea ice extents and ocean heat transports in a version of the Hadley Centre coupled model without flux adjustments. Clim Dyn 16:147–168

Gregory JM, Ingram WJ, Palmer MA, Jones GS, Stott PA, Thorpe RB, Lowe JA, Johns TC, Williams KD (2004) A new method for diagnosing radiative forcing and climate sensitivity. Geophys Res Lett 31:L03205

Hewitt SD, Broccoli AJ, Mitchell JFB, Stouffer RJ (2001) A coupled model study of the last glacial maximum: was part of the North Atlantic relatively warm? Geophys Res Lett 27:1571–1574

Johns TC, Gregory JM, Ingram WJ, Johnson CE, Jones A, Lowe JA, Mitchell JFB, Roberts DL, Sexton DMH, Stevenson DS, Tett SFB, Woodgate MJ (2003) Anthropogenic climate change for 1860 to 2100 simulated with the HadCM3 model under updated emissions scenarios. Clim Dyn 20(6):583–612

Jones GS, Gregory JM, Stott PA, Tett SFB, Thorpe RB (2005) An AOGCM simulation of the climatic response to a volcanic super-eruption. Clim Dyn 25(7–8):725–738

Knight T, Chase J (2005) Ecological succession: out of the ash. Curr Biol 15(22):R926–R927

Leavesley GH, Lusby GC, Lichty RW (1989) Infiltration and erosion characteristics of selected tephra deposits from the 1980 eruption of Mount St Helens. Hydrol Sci J (Journal Des Sciences Hydrologiques) 34(3):339–353

Lee M-Y, Chen C-H, Wei K-Y, Iizuka Y, Carey S (2004) First Toba supereruption revival. Geology 32(1):61–64

Luder T, Benz W, Stocker TF (2003) A model for long-term climatic effects of impacts. J Geophys Res 108(10-1 to 10-17). doi:10.1029/2002JE001894

Manville V (2002) Sedimentary and geomorphic responses to ignimbrite emplacement: readjustment of the Waikato River after the A.D. 181 Taupo Eruption, New Zealand. J Geol 110:519–541

Mason BG, Pyle DM, Oppenheimer C (2004) The size and frequency of the largest explosive eruptions on Earth. Bull Volcanol 66:735–748

Nammah H, Larsen FE, McCool DM, Fritts R, Molnau M (1986) Mt. St. Helens volcanic ash: effect of incorporated and unincorporated ash of two particle sizes on runoff and erosion. Agric Ecosyst Environ 15:63–72

Oppenheimer C (2002) Limited global change due to the largest known Quaternary eruption, Toba ~74kyr bp? Quat Sci Rev 21:1593–1609

Perkins ME, Nash BP (2002) Explosive silicic volcanism of the Yellowstone hotspot: the ash fall tuff record. Geol Soc Am Bull 114(3):367–381

Pollack JB, Toon OB, Sagan C, Summers A, Baldwin B, Van Camp W (1976) Volcanic explosions and climate change: a theoretical assessment. J Geophys Res 81:1071–1083

Pope VD, Gallani ML, Rowntree PR, Stratton RA (2000) The impact of new physical parameterizations in the Hadley Centre climate model—HadAM3. Clim Dyn 16:123–146

Pyle DM (1995) Mass and energy budgets of explosive volcanic eruptions. Geophys Res Lett 5:563–566

Pyle DM (2000) Sizes of volcanic eruptions. In: Sigurdsson H, Houghton BF, McNutt SR, Rymer H, Stix J (eds) Encyclopedia of volcanoes. Academic, New York, pp 263–269

Rampino M (2002) Supereruptions as a threat to civilizations on earth-like planets. Icarus 156:562–569

Rampino MR, Ambrose SH (2000) Volcanic winter in the Garden of Eden: the Toba supereruption and the Late Pleistocene human population crash. Geol Soc Am Spec Paper 345:71–82

Rampino M, Self S (1992) Volcanic winter and accelerated glaciation following the Toba super-eruption. Nature 359:50–52

Rampino M, Self S (1993) Climate-volcanism feedback and the Toba Eruption of ~74000 years ago. Quat Res 40:269–280

Reynolds RL (1975) Comparison of TRM of Yellowstone group and DRM of equivalent air-fall ash beds in western United States. Trans Am Geophys Union 56(12):977–977

Robock A (2000) Volcanic eruptions and climate. Rev Geophys 38(2):191–219

Rose WI, Chesner CA (1987) Dispersal of ash in the great Toba eruption, 75 ka. Geology 15:913–917

Savarino J, Bekki S, Cole-Dai J, Thiemens MH (2003) Evidence from sulfate mass independent oxygen isotopic compositions of dramatic changes in atmospheric oxidation following massive volcanic eruptions. J Geophys Res Atmos 108(D21):4671

Sparks RSJ, Bonnecaze R (1993) Sediment-laden gravity currents with reversing buoyancy. Earth Planet Sci Lett 114(2–3):243–257

Sparks RSJ, Walker GPL (1977) The significance of crystal-enriched air-fall ashes associated with crystal-enriched ignimbrites. J Volcanol Geotherm Res 2:329–341

Sparks RSJ, Moore JG, Rice CJ (1986) The initial giant umbrella cloud of the May 18, 1980 explosive eruption of Mount St. Helens. J Volcanol Geotherm Res 28:257–274

Sparks RSJ, Bursik MI, Carey SN, Gilbert JS, Glaze LS, Sigurdsson H, Woods AW (1997) Volcanic Plumes. Wiley, New York

Sparks RSJ, Self S, Grattan J, Oppenheimer C, Pyle DM, Rymer H (2005) Supereruptions: global effects and future threats. Geological Society of London

Stott PA, Tett SFB, Jones GS, Allen MR, Mitchell JFB, Jenkins GJ (2000) External control of 20th century temperature by natural and anthropogenic forcing. Science 290:2133–2137

Tett SFB, Jones GS, Stott PA, Hill DC, Mitchell JFB, Allen MR, Ingram WJ, Johns TC, Johnson CE, Jones A, Roberts DL, Sexton DMH, Woodgate MJ (2002) Estimation of natural and anthropogenic contributions to 20th century climate change. J Geophys Res 107:ACL 10-1 to ACL 10-24. doi:10.1029/2000JD000028

Timmreck C, Graf H-F (2005) The initial dispersal and radiative forcing of a Northern Hemisphere mid latitude super volcano: a Yellowstone case study. Atmos Chem Phys Discuss 5:7283–7308

Trenberth K (1999) Atmospheric moisture recycling: role of advection and local evaporation. J Clim 12:1368–1381

Wilson MF, Henderson-Sellers A (1985) A global archive of land cover and soils data for use in general circulation climate models. J Climatol 5(2):119–143

Witham C, Oppenheimer C, Horwell CJ (2005) Volcanic ash-leachates: a review and recommendations for sampling methods. J Volcanol Geotherm Res 141(3–4):299–326

Woods AW, Wohletz K (1991) Dimensions and dynamics of co-ignimbrite eruption columns. Nature 350:225–228

Zielinski GA, Mayewski PA, Meeker LD, Whitlow S, Twickler MS, Taylor K (1996) Potential atmospheric impact of the Toba mega-eruption ~71,000 years ago. Geophys Res Lett 23(8):837–840

Zielinski GA, Mayewski PA, Meeker LD, Gronvold K, Germani MS, Whitlow S, Twickler M, Taylor K (1997) Volcanic aerosol records and tephrochronology of the Summit, Greenland, ice cores. J Geophys Res 102(C12):26625–26640